Layer-by-Layer Doping of Few-Layer Graphene Film

Fethullah Güneş,[†,§] Hyeon-Jin Shin,[†,‡,§] Chandan Biswas,[†] Gang Hee Han,[†] Eun Sung Kim,[†] Seung Jin Chae,[†] Jae-Young Choi,[‡,*] and Young Hee Lee[†,*]

[†]BK21 Physics Division, Department of Energy Science, and Center for Nanotubes and Nanostructured Composites, Sungkyunkwan Advanced Institute of Nanotechnology, Sungkyunkwan University, Suwon 440-746, South Korea, and [‡]Display Lab, Samsung Advanced Institute of Technology (SAIT), P.O. Box 111, Suwon 440-600, South Korea. [§]These authors contributed equally to this work.

ABSTRACT We propose a new method of layer-by-layer (LbL) doping of thin graphene films. Large area monolayer graphene was synthesized on Cu foil by using the chemical vapor deposition method. Each layer was transferred on a polyethylene terephthalate substrate followed by a salt-solution casting, where the whole process was repeated several times to get LbL-doped thin layers. With this method, sheet resistance was significantly decreased up to ~80% with little sacrifice in transmittance. Unlike samples fabricated by topmost layer doping, our sample shows better environmental stability due to the presence of dominant neutral Au atoms on the surface which was confirmed by angle-resolved X-ray photoelectron spectroscopy. The sheet resistance of the LbL-doped four-layer graphene (11 × 11 cm^2) was 54 Ω/sq at 85% transmittance, which meets the technical target for industrial applications.

KEYWORDS: graphene · layer by layer doping · gold chloride · environmental stability · transparent conducting films

Carbon materials such as carbon nanotubes (CNTs), reduced graphite oxide (RGO), and graphene are good candidates for conducting films with high transmittance and excellent flexibility. One serious drawback is relatively high sheet resistance compared to that of conventional indium tin oxide (ITO). In the case of CNTs, a mixture of metallic and semiconducting CNTs in the sample creates Schottky barriers in the random network of CNT film, resulting in high contact resistance.[1−3] In the case of RGO, the presence of the remaining oxygen-related defects[4,5] and the contacts formed by the patched RGO flakes are still the main sources of high resistance, despite the prevailing two-dimensional contacts, in comparison to the point contacts of the competing CNTs. Recently, large area graphene was successfully synthesized by chemical vapor deposition (CVD).[6−10] The graphene seems to be an ideal material for flexible transparent conducting films owing to an increased mean free path of carriers caused by a decrease in the number of defects such as oxygen sites and contact between flakes in RGO. Furthermore, few-layer large area graphene with high transmittance and robust adhesion to plastic polymers without extra treatment can be realized. Nevertheless, the graphene quality is strongly dependent on the growth conditions, and low sheet resistance has not been realized because of the poor crystallinity, formation of wrinkles, and small domain sizes of graphene layers.[9]

Another approach to improve sheet resistance of the film is to use chemical doping. Since CNTs are p-type under ambient conditions, oxidizing agents and metal salts have been used for p-type doping, giving rise to an improved sheet resistance up to 90%.[11−16] The sheet resistance of RGO was also enhanced by the doping of metal salt, although the improvement reached to about 55% at high mole concentration.[17,18] The degradation of conductivity with these chemical dopants under ambient conditions has also been an issue in practical applications.[19]

In this report, we propose a new approach of layer-by-layer (LbL) doping to improve the conductivity of transparent graphene films. To realize LbL doping, a single graphene layer was synthesized on Cu foil by using CVD. Each layer was transferred to polyethylene terephthalate (PET) substrate followed by $AuCl_3$ doping. Our results demonstrate not only improvement of sheet resistance and uniformity but also better environmental stability compared to topmost layer doping. The optimized LbL-doped four-layer graphene shows a sheet resistance of 54 ohm/sq and a transmittance of 85% at 550 nm with excellent bending stability.

*Address correspondence to leeyoung@skku.edu, jaeyoung88.choi@samsung.com.

Received for review April 26, 2010 and accepted July 19, 2010.

Published online July 27, 2010.
10.1021/nn1008808

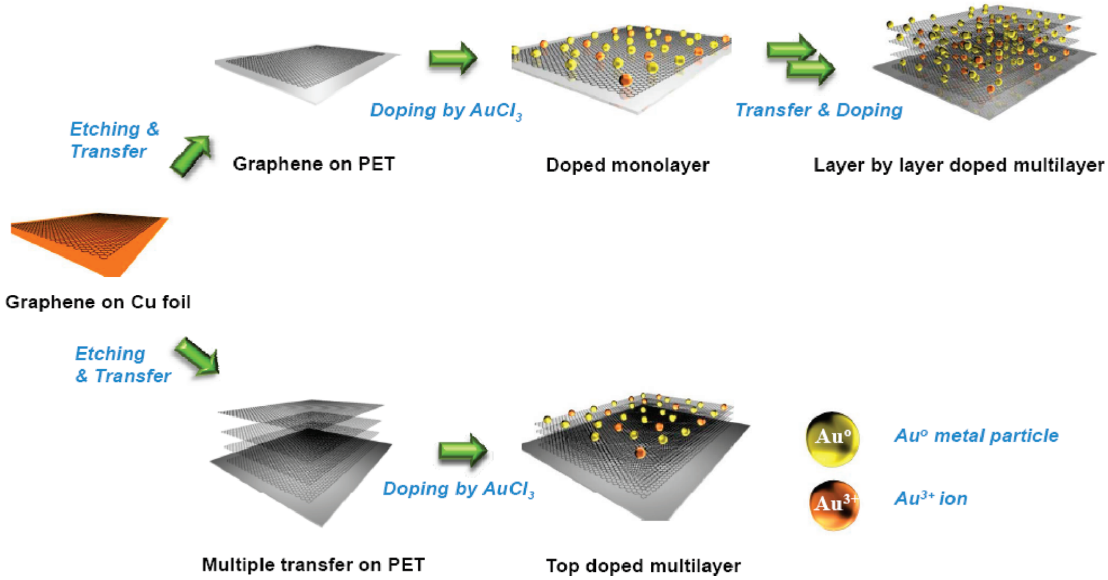

Figure 1. The schematic of the LbL-doping strategy. The top steps indicate LbL doping and the bottom steps indicate the topmost layer doping. Au atoms or ions are indicated by different colors.

RESULTS AND DISCUSSION

Figure 1 shows a schematic of LbL doping strategy. A graphene layer synthesized on Cu foil is mostly a single layer except for a small portion of bilayers and triple layers (Supporting Information, Figure S1). The average transmittance was 97.4 ± 0.3%, indicating the uniformity of the film thickness. Once the single graphene layer was transferred onto PET film, 10 mM $AuCl_3$ solution was spin-casted on it. Another graphene layer was transferred directly onto that layer followed by the similar spin-casting of $AuCl_3$ solution. This process was repeated until the films had over 80% transmittance. For comparison, we prepared four graphene layers by multiple transfers. Only the topmost layer was spin-casted with $AuCl_3$ solution in this case.

The sheet resistance and transmittance were summarized in Figure 2. The pristine single graphene sheet shows a large sheet resistance of 725 ohm/square at a transmittance of 97.6% at 550 nm (dark square). Relatively high sheet resistance is related to the less well-

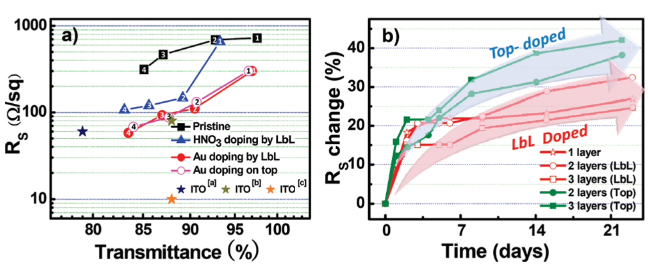

Figure 2. (a) The sheet resistance and transmittance of various samples as a function of the number of graphene layers: (■) pristine graphene layers, (▲) LbL nitric acid doping, (●) LbL Au doping, (○) the topmost layer Au doping. The numbers in the symbol indicates the number of layers. Stars indicate available ITO films (Superscripts a, b, and c are as indicated in Table 1). (b) The sheet resistance change as a function of time for various conditions: (☆) Au-doped monolayer, (○) LbL Au-doped bilayers, (□) LbL Au-doped three layers, (●) the topmost layer Au-doped two layers, (■) the topmost layer Au-doped three layers.

defined crystallinity of the film and finite domain sizes, which could be tuned during synthesis. The decrease of the sheet resistance by adding more layers was not so prominent, unlike that in the carbon nanotubes.[11] This could be ascribed to the disordered AB layer stacking and large interlayer distance which will be described later. With $AuCl_3$ doping (filled circle), the sheet resistance was greatly reduced by about 80%, regardless of the thickness, while the transmittance was slightly decreased due to the light scattering from Au nanoparticles formed during the reduction reaction.[12] These values were comparable to that of conventional ITO films.[20,21] It was observed (Figure 2, open circle) that the sheet resistance of the LbL Au-doped film was improved compared to that of the topmost layer Au-doped film (Table 1) (Supporting Information, Figure S2). On the other hand, the sheet resistances were also improved by nitric acid treatment but were still much higher than those of Au-doped films. One intriguing advantage of the LbL approach can be demonstrated in Figure 2b. The film was exposed in air for a long time to see the stability of the film after doping. The sheet resistance of the LbL-doped film was more stable than that of topmost layer-doped film.

The transmittance is calculated by

$$T = \left(1 + \frac{Z_0}{2R_s}\frac{\sigma_{op}}{\sigma_{DC}}\right)^{-2}$$

where Z_0 is impedance of free space and R_s is the sheet resistance.[22] The ratio of DC conductivity over optical conductivity (σ_{DC}/σ_{op}) was calculated as shown in Table 1. From the calculated ratio of σ_{DC}/σ_{op}, the ratio value is 21 in the pristine monolayer graphene case without doping, which is better than the reported values.[23,24] The ratio of the LbL Au-doped graphene layers reached the range of industrial requirements (σ_{DC}/σ_{op} = 35)

TABLE 1. Numerical Values of Sheet Resistance and Transmittance at 550 nm for the Graphene and ITO Films, as Shown in Figure 2a

	graphene on plastic													ITO on plastic	
	pristine			layer by layer doping						top doping				ITO on PET	
				HNO_3			$AuCl_3$			$AuCl_3$				ITO	
no. of layers	*T* %	R_s (ohm/sq)	σ_{DC}/σ_{op}	*T* %	R_s (ohm/sq)	σ_{DC}/σ_{op}	*T* %	R_s (ohm/sq)	σ_{DC}/σ_{op}	*T* %	R_s (ohm/sq)	σ_{DC}/σ_{op}		*T* %	R_s (ohm/sq)
1	97.6	725	21	93.3	657	8	96.6	301	36	96.6	301	36			
2	92.8	690	7	89.2	147	22	90.5	111	33	90.7	131	29		>88	60−100[a]
3	87.1	466	6	85.6	120	19	87.0	93	28	87.7	88	32		>88	8−12[b]
4	85.1	313	7	83.1	107	18	83.5	58	35	84.0	68	30		>79	60[c]

[a]Thickness of ITO sample = 100 nm.[20] [b]Thickness of ITO sample = 5−30 nm.[20] [c]Thickness of ITO sample = 120−160 nm.[21]

reported in the literature,[22,25] which is comparable to the maximum value of carbon nanotubes.[25,26] This value became poorer in the case of nitric-acid doped and topmost-doped graphene layers. Although LbL-doped graphene layers provided the largest values among the reported ones, it is still far smaller than the calculated value of 330.[22] This suggests that there is still room to improve defects on graphene and in the doping strategy. A large interlayer distance of more than 0.34 nm is another cause of small optical conductivity.

To understand the stability dependence, we performed angle-resolved X-ray photoelectron spectroscopy (AR-XPS). Normal XPS which includes information for all the layers (bulk) shows four peaks in the Au 4f spectrum: two Au^{3+} related peaks near 90.3 and 86.6 eV and two Au^0 peaks near 87.8 and 84.1 eV.[17] On the other hand, low angle XPS which includes mostly surface information shows remaining components of Au^0 and Au^{3+} (Figure 3). The difference in the surface structure between the LbL-doped and the top-doped film is the abundance of neutral Au atoms in the LbL-doped film. There could be several reasons for this difference. The diameter of a neutral Au atom (1.37 Å) is larger than that of a Au ion (0.85 Å), which is larger than the diameter of a benzene ring (1.05 Å). Therefore, neutral Au atoms are unlikely to penetrate into ideal sublayer graphenes and furthermore have a tendency of agglomeration to form Au clusters, as observed in SEM (Figure 3d). On the other hand, Au ions can penetrate into sublayer graphenes due to smaller sizes. In the case of LbL-doped film, the penetrated Au ions still remain unchanged because the sublayer graphene is already doped and saturated. This provides more abundant Au ions in the bulk in the LbL-doped film (Figure 3a). In the case of top-doped film, however, Au ions penetrated into sublayers are further reduced to neutral Au atoms by accepting electrons from underneath undoped graphene layers. This is evidenced by the lower Au ion peak intensity in Figure 3b in the bulk of top-doped film. Au atoms and ions were equally probable in all of the layers, that is, no dominant neutral Au atoms were observed in the bottom layer, as can be seen in Figure 3b. This strongly suggests that not only Au ions but also neutral Au atoms are likely to penetrate through presumable preexisting defects such as vacancies and dislocation lines that have much larger sizes.

The presence of dominating neutral Au^0 on the surface of LbL-doped film makes it hydrophobic. This hydrophobicity could be ascribed to a source of high environmental stability shown in Figure 2b. The presence of neutral Au atoms at the outmost surface also acts as a protective layer for the inner Au ions. In the case of topmost-layer doping of four-layer film (Figure 3b), Au peaks were still visible from bulk at normal XPS, suggesting that Au ions or atoms are penetrated into the bulk even in the case of topmost layer doping. This implies why the difference in the sheet resistance between LbL-doped four layer film and topmost-doped four layer film was not so obvious. It is not clearly understood how Au ions or neutral Au atoms are incorporated into the bulk. It could be associated with plausible defects formed in the CVD-grown graphene. Again by arranging the XPS data together for surfaces of LbL-doped four-layer film, topmost-doped four-layer film, and single layer-doped film (Figure 3c), one can clearly

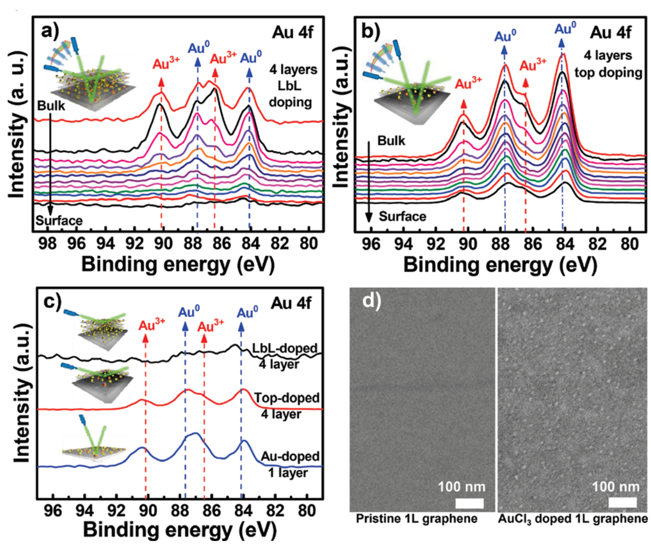

Figure 3. Au 4f angle-resolved X-ray photoelectron spectroscopy for (a) LbL-doped four-layer film and (b) topmost layer-doped four-layer film. (c) X-ray photoelectron low angle-spectra for LbL-doped four layer film (top), low angle-spectra for top-doped four layer film (middle), and normal-spectra for Au-doped monolayer film (bottom). (d) SEM images for pristine (left) and doped single layer film (right).

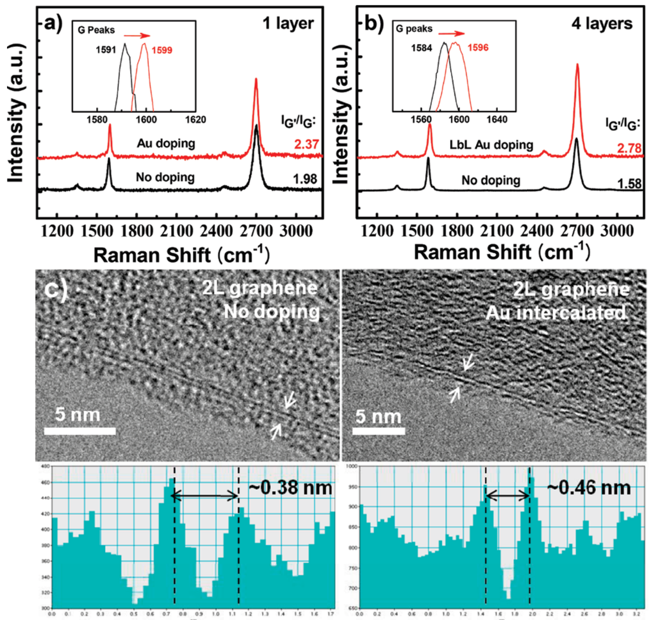

Figure 4. Raman spectra of (a) $AuCl_3$-doped (top) and pristine (bottom) monolayer graphene film, and (b) $AuCl_3$-doped (top) and pristine (bottom) four-layer graphene film. The ratio of G′ band intensity to G band intensity is given on the right sides of each plot. All the peaks were normalized by the G-band intensity. (c) HR-TEM images of undoped bilayer graphene (left) and bilayer graphene with $AuCl_3$ doping (right). Arrows indicate the position of intensity profile obtained on the edge lines shown in the bottom panel. Note that the scale bar is different in the panels.

see that neutral Au^0 is dominant in the top layer in the case of LbL-doped four-layer film, whereas topmost-layer-doped four-layer film and single-layer doped film showed mixed Au^{3+} and Au^0. In this sense, stability is best in the LbL-doped film. Au clusters were formed during Au reduction (Figure 3d).

To understand the doping effect, we took Raman spectroscopy on graphene films. It is well-known that the peak position of G band changes depending on the doping effect. In the case of p-type doping, the G band position upshifts due to the phonon stiffening effect by charge extraction.[13,27] In Au-doped monolayer graphene case (Figure 4a), the G band has shifted about 8 cm^{-1} from 1591 (pristine graphene) to 1599 cm^{-1} (Au-doped graphene). The peak shift (12 cm^{-1}) was more prominent in the case of four-layer LbL doping (Figure 4b). Another intriguing phenomenon is the intensity ratio of G′ band to G band. Highly degenerate p-type doping increases metallicity of the Au-doped CNT films.[13] In the case of graphene, however, the G′ band intensity decreases after doping, independent of dopant types.[28−30] In our case of monolayer graphene, the intensity ratio $I_{G'}/I_G$ increased slightly after doping. The increase of the ratio was more prominent in the case of four layers. This is good contrast with the previous reports.[28−30] This difference could be ascribed to the use of different samples (highly oriented pyrolytic graphite). High-resolution transmission electron microscopy (HR-TEM) images in Figure 4c show the double-line at the edge of the bilayer graphene prepared by LbL method without and with $AuCl_3$ doping. Interlayer distances of the pristine bilayer graphene and Au intercalated bilayer graphene were obtained from the intensity profile of the lines at the edges as shown in the bottom panels of the figure. Intensity profiles show that the interlayer distance was extended to nearly 3.8 Å, in the case of undoped graphene, and to nearly 4.6 Å in the case of $AuCl_3$-doped bilayer graphene, compared to 3.4 Å of graphite.[31] The interlayer expansion with doping was expected because of the presence of Au cluster formation, as shown in Figure 3d. This weakly bound interlayer could be a reason why the sheet resistance saturates at four layers.

Figure 5 demonstrates the bending stability of doped graphene films. Conventionally, ITO is a material used for transparent electrode applications. However, it is not compatible for flexible electronics where it can easily be deteriorated at bending. The force was applied to create 1% strain where the strain is defined as $\varepsilon = t/2r \times 100$ (%); t is the film thickness (100 μm), and r is the bending radius (5 mm). Typical 1% strain is illustrated in the right inset of Figure 5. The bending was repeated for 1000 times with a frequency of 1 Hz. After 1000 cycles of bending, the sheet resistance of LbL-doped four-layer film changed by 16.3%, which is similar to that of the pristine four-layer film. However, the sheet resistance of HNO_3-doped four-layer film was changed by 24.2%, which is higher than that of other films. This indicates LbL doping did not change the mechanical properties much, although small Au clusters of sizes of less than 10 nm were formed on the film. Therefore, this robust mechanical property could be applied for developing stretchable touch panel displays.

CONCLUSION

We developed a new method of layer-by-layer $AuCl_3$ doping to decrease the sheet resistance of graphene films and to improve environmental stability. Although

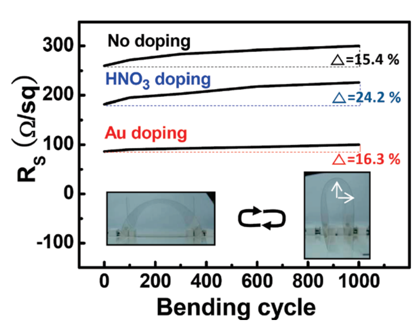

Figure 5. Bending stability test results for four-layer pristine (top), HNO_3-doped (middle), and Au-doped (bottom) graphene films. Bending morphology is illustrated in the inset. Graphene film on 100 μm thick PET substrate was bent with 5.0 mm radius for 1000 times at a frequency of 1 Hz.

the concept was demonstrated with graphene films in sizes of 11 × 11 cm^2 with low sheet resistance of 54 ohm/square and a transmittance of 85% at 550 nm, this method can be generalized to a uniform large area graphene film which is suitable for large size displays. The prepared graphene film shows superior performance in flexibility and stretchability compared to conventional ITO-based transparent conducting films. The performance of our graphene films can further be improved by reducing defects and damage formation during synthesis and transfer processes to meet requirements of different applications such as LCDs, thin film solar cells, flexible touch screen panels and electronic papers.

EXPERIMENTAL SECTION

Preparation of Single-Layer Graphene Film. Large area monolayer graphene films were synthesized on Cu foil by the CVD method. Cu foil of 85 × 75 cm^2 with a thickness of 70 μm was rolled into a vacuum CVD quartz chamber. The temperature was increased up to 950 °C in H_2 atmosphere and the foil was annealed for 1 h at this temperature prior to growth. Graphene was synthesized at 950 °C by a gas flow of H_2/CH_4, 80/250 sccm, for 20 min, and then the chamber was cooled down to room temperature in the same atmosphere. After synthesis, the Cu foil was cut into equal small pieces (3 × 3 cm^2), coated with PMMA, and immersed into Cu etchant ($FeCl_3$) solution in order to etch away the Cu foil. When Cu was completely etched away, the graphene sheets with PMMA were rinsed in deionized water several times to wash away etchant residues. Then, PMMA-coated graphene sheets were transferred onto a PET substrate. PMMA was removed by acetone after graphene was completely adhered onto the substrate.

Layer-by-Layer Doping with $AuCl_3$. Gold chloride ($AuCl_3$) powder was purchased from Sigma-Aldrich. A 10 mM $AuCl_3$ solution was prepared by dissolving $AuCl_3$ powder in nitromethane followed by sonication for 5 min. The 10 mM $AuCl_3$ solution was then dropped on the graphene film by a micropipet and spin-coated at 2000 rpm for 1 min after a 30 s residual time.

These steps were repeated several times on the same graphene-coated substrate in order to maintain LbL doping of graphene sheets up to four layers. For comparison, graphene layers without doping up to four layers were also transferred, and then only the topmost layer was doped by $AuCl_3$. A LbL doping approach with a nitric acid solution of 50% in deionized water was used as another dopant.

Characterizations. Sheet resistance measurements were performed by a four-point method (Keithley 2000 multimeter) at room temperature. UV−vis−NIR absorption spectroscopy (Varian, Cary 5000) and Raman spectroscopy (Renishaw, RM-1000 Invia) with excitation energy of 2.41 eV (514 nm, Ar+ ion laser) were used for characterizing the optical properties of the graphene films on PET and SiO_2/Si substrates, respectively. The angle-resolved XPS spectrometry (QUANTUM 2000, Physical electronics, USA) was performed using focused monochromatized Al Kα radiation (1486.6 eV) in order to determine the atomic ratios of Au^{3+} to Au^0 and nondestructive depth profile of graphene films. HR-TEM (JEM 2100F, JEOL) was used to investigate the interlayer distance of bilayer graphene before and after Au particle intercalation. Samples for HR-TEM were prepared on SiO_2/Si substrates as described before and then directly transferred onto Cu grids by etching the SiO_2 layer in diluted HF acid solution and then further dilution.

Acknowledgment. This work was supported by the MOE through the STAR-faculty project, TND project, WCU(World Class University) program through the KOSEF funded by the MEST (R31-2008-000-10029-0), the KICOS through a grant provided by MOST in 2007 (No. 2007-00202), and KOSEF through CNNC at SKKU.

Supporting Information Available: The optical image of graphene film transferred on 300 nm SiO_2/Si wafer and the transmittance of the monolayer graphene film synthesized on Cu foil and transferred on 100 μm PET substrate; photographs of graphene films transferred on PET substrate with different number of layers and different doping methods. This material is available free of charge *via* the Internet at http://pubs.acs.org.

REFERENCES AND NOTES

1. Fuhrer, M. S.; Nygard, J.; Shih, L.; Forero, M.; Yoon, Y.-G.; Mazzoni, M. S. C.; Choi, H. J.; Ihm, J.; Louie, S. G.; Zettl, A.; *et al*. Crossed Nanotube Junctions. *Science* **2000**, *288*, 494–497.
2. Miyata, Y.; Yanagi, K.; Maniwa, Y.; Kataura, H. Highly Stabilized Conductivity of Metallic Single Wall Carbon Nanotube Thin Films. *J. Phys. Chem. C* **2008**, *112*, 3591–3596.
3. Blackburn, J. L.; Barnes, T. M.; Beard, M. C.; Kim, Y.-H.; Tenent, R. C.; McDonald, T. J.; To, B.; Coutts, T. J.; Heben, M. J. Transparent Conductive Single-Walled Carbon Nanotube Networks with Precisely Tunable Ratios of Semiconducting and Metallic Nanotubes. *ACS Nano* **2008**, *2*, 1266–1274.
4. Shin, H.-J.; Kim, K. K.; Benayad, A.; Yoon, S.-M.; Park, H. K.; Jung, I.-S.; Jin, M. H.; Jeong, H.-K.; Kim, J. M.; Choi, J.-Y.; *et al*. Efficient Reduction of Graphite Oxide by Sodium Borohydride and Its Effect on Electrical Conductance. *Adv. Funct. Mater.* **2009**, *19*, 1987–1992.
5. Schniepp, H. C.; Li, J.-L.; McAllister, M. J.; Sai, H.; Herrera-Alonso, M.; Adamson, D. H.; Prud'homme, R. K.; Car, R.; Saville, D. A.; Aksay, I. A. Functionalized Single Graphene Sheets Derived from Splitting Graphite Oxide. *J. Phys. Chem. B* **2006**, *110*, 8535–8539.
6. Reina, A.; Jia, X.; Ho, J.; Nezich, D.; Son, H.; Bulovic, V.; Dresselhaus, M. S.; Kong, J. Large Area, Few-Layer Graphene Films on Arbitrary Substrates by Chemical Vapor Deposition. *Nano Lett.* **2009**, *9*, 30–35.
7. Kim, K. S.; Zhao, Y.; Jang, H.; Lee, S. Y.; Kim, J. M.; Kim, K. S.; Ahn, J.-H.; Kim, P.; Choi, J.-Y.; Hong, B. H. Large-Scale Pattern Growth of Graphene Films for Stretchable Transparent Electrodes. *Nature* **2009**, *457*, 706–710.
8. Güneş, F.; Han, G. H.; Kim, K. K.; Kim, E. S.; Chae, S. J.; Park, M. H.; Jeong, H.-K.; Lim, S. C.; Lee, Y. H. Large-Area Graphene-Based Flexible Transparent Conducting Films. *NANO* **2009**, *4*, 83–90.
9. Chae, S. J.; Güneş, F.; Kim, K. K.; Kim, E. S.; Han, G. H.; Kim, S. M.; Shin, H.-J.; Yoon, S.-M.; Choi, J.-Y.; Park, M. H.; *et al*. Synthesis of Large-Area Graphene Layers on Poly-Nickel Substrate by Chemical Vapor Deposition: Wrinkle Formation. *Adv. Mater.* **2009**, *21*, 2328–2333.
10. Li, X.; Cai, W.; An, J.; Kim, S.; Nah, J.; Yang, D.; Piner, R.; Velamakanni, A.; Jung, I.; Tutuc, E.; *et al*. Large-Area Synthesis of High-Quality and Uniform Graphene Films on Copper Foils. *Science* **2009**, *324*, 1312–1314.
11. Geng, H.-Z.; Kim, K. K.; So, K. P.; Lee, Y. S.; Chang, Y.; Lee, Y. H. Effect of Acid Treatment on Carbon Nanotube-Based Flexible Transparent Conducting Films. *J. Am. Chem. Soc.* **2007**, *129*, 7758–7759.
12. Kim, K. K.; Bae, J. J.; Park, H. K.; Kim, S. M.; Geng, H.-Z.; Park, K. A.; Shin, H.-J.; Yoon, S.-M.; Benayad, A.; Choi, J.-Y.; *et al*. Fermi Level Engineering of Single-Walled Carbon Nanotubes by $AuCl_3$ Doping. *J. Am. Chem. Soc.* **2008**, *130*, 12757–12761.
13. Kim, K. K.; Bae, J. J.; Kim, S. M.; Park, H. K.; An, K. H.; Lee, Y. H. Control of P-Doping on Single-Walled Carbon Nanotubes with Nitronium Hexafluoroantimonate in Liquid Phase. *Phys. Status Solidi B* **2009**, *246*, 2419–2422.

14. Shin, H.-J.; Kim, S. M.; Yoon, S.-M.; Benayad, A.; Kim, K. K.; Kim, S. J.; Park, H.-K.; Choi, J.-Y.; Lee, Y. H. Tailoring Electronic Structures of Carbon Nanotubes by Solvent with Electron-Donating and -Withdrawing Groups. *J. Am. Chem. Soc.* **2008**, *130*, 2062–2066.
15. Yoon, S.-M.; Kim, S. J.; Shin, H.-J.; Benayad, A.; Choi, S. J.; Kim, K. K.; Kim, S. M.; Park, Y. J.; Kim, G.; Choi, J.-Y.; *et al.* Selective Oxidation on Metallic Carbon Nanotubes by Halogen Oxoanions. *J. Am. Chem. Soc.* **2008**, *130*, 2610–2616.
16. Liu, X. M.; Romero, H. E.; Gutierrez, H. R.; Adu, K.; Eklund, P. C. Transparent Boron-Doped Carbon Nanotube Films. *Nano Lett.* **2008**, *8*, 2613–2619.
17. Benayad, A.; Shin, H.-J.; Park, H. K.; Yoon, S.-M.; Kim, K. K.; Jin, M. H.; Jeong, H.-K.; Lee, J. C.; Choi, J.-Y.; Lee, Y. H. Controlling Work Function of Reduced Graphite Oxide with Au-Ion Concentration. *Chem. Phys. Lett.* **2009**, *475*, 91–95.
18. Kong, B.-S.; Geng, J.; Jung, H.-T. Layer-by-Layer Assembly of Graphene and Gold Nanoparticles by Vacuum Filtration and Spontaneous Reduction of Gold Ions. *Chem. Commun.* **2009**, 2174–2176.
19. Kim, K. K.; Reina, A.; Shi, Y.; Park, H.; Li, L.-J.; Lee, Y. H.; Kong, J. Enhancing the Conductivity of Transparent Graphene Films *via* Doping. *Nanotechnology* **2010**, *21*, 285205.
20. These products are commercially available *via* the Internet: http://www.2spi.com/catalog/standards/ITO-coated-slides-resistivities5.html.
21. These products are commercially available *via* Internet: http://www.sigmaaldrich.com.
22. De, S.; Coleman, J. N. Are There Fundamental Limitations on the Sheet Resistance and Transmittance of Thin Graphene Films. *ACS Nano* **2010**, *4*, 2713–2720.
23. Cai, W.; Zhu, Y.; Li, X.; Piner, R. D.; Ruoff, R. S. Large Area Few-Layer Graphene/Graphite Films as Transparent Thin Conducting Electrodes. *Appl. Phys. Lett.* **2009**, *95*, 123115.
24. Li, X.; Zhu, Y.; Cai, W.; Borysiak, M.; Han, B.; Chen, D.; Piner, R. D.; Colombo, L.; Ruoff, R. S. Transfer of Large-Area Graphene Films for High-Performance Transparent Conductive Electrodes. *Nanolett.* **2009**, *9*, 4359–4363.
25. Nirmalraj, P. N.; Lyons, P. E.; De, S.; Coleman, J. N.; Boland, J. J. Electrical Connectivity in Single-Walled Carbon Nanotube Networks. *Nanolett.* **2009**, *9*, 3890–3895.
26. Wu, Z.; Chen, Z.; Du, X.; Logan, J. M.; Sippel, J.; Nikolou, M.; Kamaras, K.; Reynolds, J. R.; Tanner, D. B.; Hebard, A. F.; Rinzler, A. G. Transparent, Conductive Carbon Nanotube Films. *Science* **2004**, *305*, 1273–1276.
27. Rao, A. M.; Eklund, P. C.; Bandow, S.; Thess, A.; Smalley, R. E. Evidence for Charge Transfer in Doped Carbon Nanotube Bundles from Raman Scattering. *Nature* **1997**, *388*, 257–259.
28. Das, A.; Pisana, S.; Chakraborty, B; Piscanec, S.; Saha, S. K.; Waghmare, U. V.; Novoselov, K. S.; Krishnamurthy, H. R.; Geim, A. K.; Ferrari, A. C.; *et al.* Monitoring Dopants by Raman Scattering in an Electrochemically Top-Gated Graphene Transistor. *Nat. Nanotechnol.* **2008**, *3*, 210–215.
29. Dong, X.; Fu, D.; Fang, W.; Shi, Y.; Chen, P.; Li, L.-J. Doping Single-Layer Graphene with Aromatic Molecules. *Small* **2009**, *5*, 1422–1426.
30. Voggu, R.; Das, B.; Rout, C. S.; Rao, C. N. R. Effects of Charge Transfer Interaction of Graphene with Electron Donor and Acceptor Molecules Examined Using Raman Spectroscopy and Cognate Techniques. *J. Phys.: Condens. Matter* **2008**, *20*, 472204.
31. Malesevic, A.; Vitchev, R.; Schouteden, K.; Volodin, A.; Zhang, L.; Tendeloo, G. V.; Vanhulsel, A.; Haesendonck, C. V. Synthesis of Few-Layer Graphene *via* Microwave Plasma-Enhanced Chemical Vapour Deposition. *Nanotechnology* **2008**, *19*, 305604.